AIP Publishing
Applied Physics Letters
ACCEPTED MANUSCRIPT
This is the author's peer reviewed, accepted manuscript. However, the online version of record will be different from this version once it has been copyedited and typeset.
PLEASE CITE THIS ARTICLE AS DOI: 10.1063/5.0205876

Electric field control of the energy gap in ZnO and $BaSnO_3$ films grown on PMN-PT

G. Bridoux,[1,*] G. A. Mogensen,[2] G. Nieva,[2] J. Guimpel,[2] J. M. Ferreyra,[1] M. R. Tolosa,[1] and M. Villafuerte[1]

[1] *Laboratorio de Física del Sólido, INFINOA (CONICET-UNT), Facultad de Ciencias Exactas y Tecnología, Universidad Nacional de Tucumán, 4000 San Miguel de Tucumán, Argentina*

[2] *Laboratorio de Bajas Temperaturas, Centro Atómico Bariloche and Instituto Balseiro, Instituto de Nanociencia y Nanotecnología (CNEA - CONICET), Nodo Bariloche, 8400 S. C. Bariloche, Argentina*

(Dated: June 3, 2024)

ZnO and $BaSnO_3$ (BSO) thin films grown on $Pb(Mg_{1/3}Nb_{2/3})O_3$-$PbTiO_3$ (PMN-PT) substrates have been studied using electrical resistance and photoconductivity spectra measurements under different applied electric fields on the substrate. The behavior of the resistance and the energy gap (E_G) extracted from the photoconductivity (PC) spectra are modified by the polarization state of the substrate in the case of the ZnO film while for BSO these physical parameters depend on the strain imposed by the substrate when a voltage is applied on the PMN-PT. In the latter case, an in-plane tensile (compressive) strain leads to a reduction (increase) of the resistance and the energy gap when an external electric field is applied on the substrate. The behavior of ZnO and BSO can be explained by the different crystalline structure in both films and by the fact that ZnO is also a piezoelectric material. In ZnO a change in the polarization state of the substrate is associated with an imposed strain and an induced polarization on the film that leads to a modification of the band bending and hence of the energy gap. In the case of BSO, a shift of the impurity and conduction band generates a modification of the energy gap for the different types of strain.

In the last twenty years there has been renewed interest in oxide bearing compounds and transition metal oxides (TMO) [1–3] due to a significant advance in the fabrication techniques of thin films and low dimensional structures [4, 5]. The main advantages of these compounds reside in their earth-abundance and multi-functionality [6], which make them a complementary candidate to silicon for technological applications [7, 8]. On the other side, one of the challenges that emerges on these materials is the presence of intrinsic defects (mainly oxygen vacancies) due to their low formation energy [9–11]. In fact, the low electron mobility [11–13] and some of the effects observed at the interfaces between these types of layers [6] can be related to the presence of defects or residual strain.

Ferroelectric-piezoelectric materials based on these oxides like $BiFeO_3$ [14, 15], $BaTiO_3$ [16–18], PZT [19, 20], HfO [21, 22], $HfZrO_x$ [23–25], PMN-PT [26, 27] caught the attention in the last decade due to the influence that polarization and/or strain induced by an applied voltage or electric field can have on the properties of films grown or transferred to them [26, 27]. In particular, PMN-PT single crystals have been widely used as a building block or substrate for growing different types of thin films with this goal [26–29, 32–35]. Despite of that, the exploration of optoelectronic properties of thin films on PMN-PT is rather scarce [36–38]. In this regard, the present work study the photoconducting properties of ZnO and BSO on PMN-PT, two wide band gap semiconductors which are appealing TMO materials due to its polar character and piezoelectric properties [39, 40] (in the case of ZnO), and the high electron mobility values achieved with lanthanum doping [41–43] which is the case of BSO.

ZnO and BSO films were grown on one-side-polished [001] PMN-PT single crystals substrates (dimensions: 5 x 5 x 0.5 mm^3) by pulsed laser deposition (PLD) using a Nd:YAG laser operated at a wavelength of 266 nm and a repetition rate of 10 Hz. ZnO film was grown at $T = 300\,°C$ with an oxygen pressure of 0.1 mTorr and laser fluence of $F = 1.9\,J\,cm^{-2}$ with a resulting thickness of $t = 50\,nm$. For the BSO film, an insulating buffer layer of BSO using 1500 pulses, $P_{O_2} = 60\,mTorr$ and $F = 1.8\,J\,cm^{-2}$ was deposited before the deposition of the semiconducting BSO film employing 6000 pulses, $P_{O_2} = 1\,mTorr$ and $F = 1.5\,J\,cm^{-2}$ in order to prevent the Pb diffusion towards this layer since the growth temperature was $T = 700\,°C$ in this case. The total thickness of the film was ∼120 nm determined from low angle x-ray reflectivity and ellipsometry. A ToF-SIMS study (Time of Flight- Secondary Ion Mass Spectroscopy) has shown that there is no diffusion of Pb to the semiconducting BSO film. This finding was also confirmed by a Rütherford Back-Scattering (RBS) study.

Fig. 1 shows the $\theta - 2\theta$ XRD pattern for both films. In the case of the ZnO film two samples have been fabricated. In one of them (sample 1), see Fig. 1a, only a small contribution of the (002) reflection can be identified which is expected due to the poor lattice matching between ZnO and the PMN-PT substrate. Moreover, an additional reflection corresponding to the (103) plane can be observed. Hence, this ZnO film is only partially oriented along the c axis. From these two reflections the in-plane lattice parameter can be extracted obtaining $a = (3.15 \pm 0.09)$Å while in bulk single crystals previous works report $a = (3.2482 \pm 0.0002)$Å [44]. The XRD pattern for the other ZnO sample (sample 2), see inset

* gbridoux@herrera.unt.edu.ar

AIP Publishing
Applied Physics Letters
ACCEPTED MANUSCRIPT
This is the author's peer reviewed, accepted manuscript. However, the online version of record will be different from this version once it has been copyedited and typeset.
PLEASE CITE THIS ARTICLE AS DOI: 10.1063/5.0205876

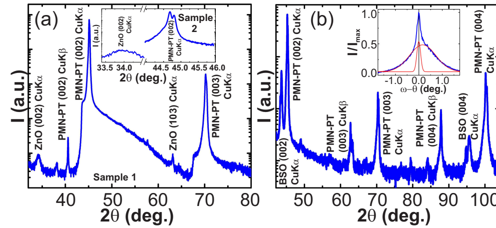

Figure 1. X-ray diffraction patterns for ZnO (sample 1) (a) and BSO films (b) on PMN-PT substrates. The inset of (a) shows the intensity comparison of the ZnO (002) peak with that of the PMN-PT substrate for another sample with no (103) peak (sample 2). The inset of (b) shows the ω-scan around the (002) peak of BSO (blue). By fitting these data with a two-peak function (red), the sharp peak can be identified as a contribution of the (002) reflection of PMN-PT (with a FWHM of $\sim 0.2^0$) while the wider peak is due to the (002) reflection of BSO (FWHM of $\sim 1.3^0$). In the case of ZnO no rocking curve generated from the film could be observed above the noise at the (002) peak position.

of Fig. 1a, shows that the (002) contribution is reduced and broader in comparison to the first sample and the (103) reflection is not observable. In the following, we will present the results corresponding to sample 2, although we have obtained similar results for sample 1.

On the other hand, the $\theta-2\theta$ XRD pattern of the BSO film (Fig. 1b) only shows sizable contributions of the (002) and (004) reflections indicating that the film has epitaxially grown in the [001] direction with cubic structure. From these reflections, an out-of plane lattice parameter value of $c = (4.1746 \pm 0.0007)$Å can be extracted, while the in-plane lattice parameter can be obtained from the Poisson's formula: $\epsilon_{zz} = -2\nu\epsilon_{xx}/(1-\nu)$, where ϵ_{zz} and ϵ_{xx} are the out-of plane and in-plane strain respectively and ν is the Poisson's ratio which takes the value $\nu = 0.23$ [45]. Considering that the lattice parameter of cubic BSO single crystals is (4.1165 ± 0.0005)Å [46] we obtain an in-plane lattice parameter of (4.019 ± 0.002)Å for our BSO film. This reduction in comparison to the bulk value of BSO is consistent with an in-plane compressive strain which is necessary to match the lattice parameter of PMN-PT ((4.0279 ± 0.0001)Å, obtained from the PMN-PT reflections, see Fig. 1b). The inset of Fig. 1b shows the ω-scan around the (002) peak of the BSO film (blue). As it can be observed, there are two contributions which can be analyzed by fitting these data with a two-peak function (red). The sharp peak has a full width at half maximum (FWHM) value of $\sim 0.2^0$ which coincides with the value obtained in a ω-scan around the (002) peak of the PMN-PT substrate. The wider peak corresponds to the contribution of the (002) reflection of the BSO film which gives a FWHM value of $\sim 1.3^0$, indicative of a highly oriented film.

The sketch of Fig. 2b shows the configuration em-

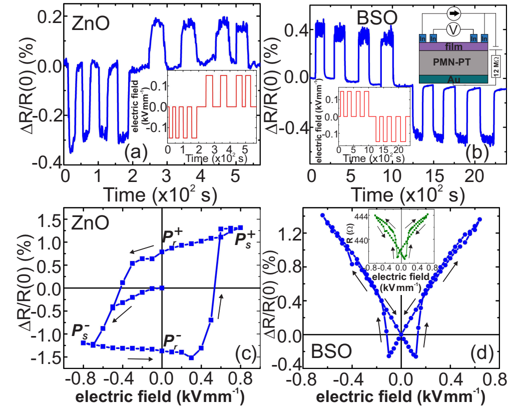

Figure 2. The electrical resistance response of ZnO (a) and BSO (b) to a sequence of electric fields (inset) applied on the PMN-PT substrate is shown. A sketch of the configuration employed for electrical resistance measurements and for the application of the electric field is also shown. We have used indium dot contacts of ~ 0.5 mm of diameter. The electrical resistance response of ZnO (c) and BSO (d) to a closed cycle sequence of applied electric field is also shown. The inset shows the same response for BSO without the subtraction of the offset at zero electric field.

ployed for the electrical resistance measurements on the film [47, 48] under an applied electric field on the PMN-PT substrate [26]. Fig. 2a and b show the time dependent electrical resistance response of the ZnO and BSO film respectively under a sequence of electric fields pulses of $\pm 0.15\,\mathrm{kV\,mm^{-1}}$. These electric field pulses values are below the coercive field of the substrate and the PMN-PT is in the unpolarized state. For both films, the electrical resistance increases (decreases) for positive (negative) electric fields [28, 30]. At $0.15\,\mathrm{kV\,mm^{-1}}$, the relative change of resistance, $\Delta R/R(0) = (R - R(0))/R(0)$, are $\sim 0.25\,\%$ and $\sim 0.4\,\%$ for ZnO and BSO respectively.

Fig. 2c and d show the electrical resistance response under a closed-cycle sequence of electric field. These experiments were performed applying pulses (as in Fig. 2a and b) of different amplitudes although a protocol applying continuous voltage leads to the same results. For ZnO (Fig. 2c) the electrical resistance follows the behavior of the polarization vs electric field curve of the PMN-PT ferroelectric [30]. Starting from the unpolarized state at zero electric field, P^0, the resistance gradually decreases as the electric field is increased towards negative values, until the negative coercive field is reached, where the resistance decreases until it reaches a saturation value (P_S^- state). If in this state the electric field is diminished, the resistance remains close to the saturation value even at zero electric field (remanent state P_r^-) until the positive coercive field is reached and the resistance is flipped to the saturation value (P_S^+). In contrast, for BSO, the elec-

AIP Publishing
Applied Physics Letters
ACCEPTED MANUSCRIPT
This is the author's peer reviewed, accepted manuscript. However, the online version of record will be different from this version once it has been copyedited and typeset.
PLEASE CITE THIS ARTICLE AS DOI: 10.1063/5.0205876

trical resistance follows a behavior similar to that of the strain vs electric field curve of the PMN-PT ferroelectric [28], see inset of Fig. 2d. After an initial decrease when the electric field is increased, the resistance starts to increase as the coercive field is reached and then it linearly increases as the electric field is increased. This curve becomes more symmetric when it is plotted in terms of $\Delta R/R(0)$ (see main panel of Fig. 2d), revealing a residual contribution of the offset resistance after the electric field is removed which probably comes from the polarization of the PMN-PT substrate [28]. The different response observed in ZnO and BSO resides in the different crystal structure obtained for both films, see Fig. 1. While in ZnO there is not a clear crystal orientation and the lattice matching between film and substrate is poor, in the case of BSO an epitaxial film was obtained with a good matching between film and substrate. This makes the latter film more sensitive to the strain imposed by the PMN-PT substrate when an electric field is applied. However, the ZnO film can still be receptive to the imposed strain and to induce a polarization, P_i^{ZnO}, via the piezoelectric effect that affects its electrical resistance [40]. It is also worth to notice that different coercive fields are obtained in Fig. 2c and d. It was checked that it is due to the different thermal annealing at which the PMN-PT substrates are subject during the fabrication of the ZnO and BSO films.

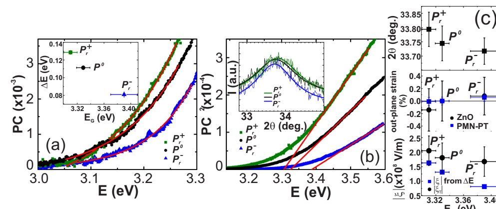

Figure 3. (a) PC spectra of ZnO at different polarization states of the PMN-PT substrate. The red curves are corresponding fits using an exponential function. (b) PC^2 spectra of ZnO at different polarization states of the PMN-PT substrate. The red lines are linear fits to these curves. The inset of (a) shows the ΔE values extracted from the fits of (a) vs the corresponding E_G values obtained from (b). The inset of (b) shows the (002) peak of ZnO at different polarization states. The curves are corresponding fits to the data. (c) ZnO (002) peak position (top); extracted out-of-plane strain for ZnO (black dots) and PMN-PT (blue squares) (central) and comparison of electric fields (in absolute value): ξ_T (extracted from P_T^{ZnO}) and ξ (extracted from ΔE) (bottom) at the different polarization states of the substrate as a function of E_G. The error bars size corresponding to the ξ values is similar to the size of the used symbols.

Photoconductivity spectra, defined as $PC = (R^{-1} - R_{dark}^{-1})/R_{dark}^{-1}$, were measured for both films. Since both films have a direct energy gap, E_G, [49, 50] and assuming that PC is proportional to the optical absorption coefficient, the linear relation $PC^2 \propto E - E_G$ should be satisfied in the proximity of the absorption onset and E_G can be extracted [51, 52]. Since both resulting films have a residual in-plane compressive strain, the obtained E_G values are higher [53, 54] compared to previously reported ones [49, 50, 55]. Taking into account the behavior of the electrical resistance under an electric field on the PMN-PT substrate, we have performed a PC spectrum at each polarization state in the case of the ZnO film: unpolarized (P^0) and remanent polarized states (P_r^+ and P_r^-). As it can be observed, the PC and PC^2 spectra onsets (Fig. 3a and b respectively) are shifted to lower energy values as the polarization state is changed from P_r^- to P^0 and P_r^+.

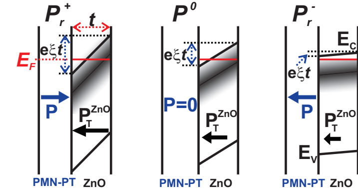

Figure 4. Sketch of the energy diagram for ZnO. A spontaneous polarization on the film ($P_T^{ZnO} = P_{esp}^{ZnO}$) generates an initial band bending in the ZnO film in the P^0 state of the PMN-PT substrate (central panel) which tilts the border of the conduction and valence band (E_C and E_V respectively) and also the impurity band (blurred black area) in an energy $e\xi t$. In the P_r^+ state (left panel), the total polarization of ZnO is increased in quantity $d_{33}\epsilon_{zz}$ in relation to the P^0 state, increasing the band bending and reducing E_G in comparison to the P^0 state. Finally, in the P_r^- state (right panel), P_T^{ZnO} is decreased in a quantity $d_{33}\epsilon_{zz}$ in comparison to the P^0 state, reducing in this way the band bending and increasing E_G. In all the cases, the Fermi energy level remains unchanged.

In ZnO it is well known that band bending due to an electric field ξ produced by surface charge or by the presence of an internal dipolar moment has an important effect in reducing the energy gap due to the Franz-Keldysh effect [40, 47, 56, 57]. In this regard, Dow and Redfield [58] proposed an exponential dependence of the absorption onset: $PC \propto e^{E/\Delta E}$, where ΔE is a measure of the strength of this internal electric field, ξ, and it is related to ΔE via $\xi = ((3\Delta E/2)m^{*1/3})^{3/2}/e\hbar$ [47, 52], where $\hbar$ is the reduced Planck constant, e and m^* are the charge and the effective mass of the electron respectively. Fig. 3a also presents the exponential fittings of the PC curves, and the ΔE values obtained for each curve are plotted against the corresponding E_G values extracted from the PC^2 spectra of Fig. 3b (see inset of Fig. 3a). As it can be observed, E_G is reduced as the polarization state is varied from P_r^- to P^0 and P_r^+ and this reduction is concomitant with a corresponding increase of ΔE suggesting that band bending generated by an increased internal polarization in the ZnO is responsible for this effect.

In order to corroborate that, the inset of Fig. 3b

AIP Publishing
Applied Physics Letters ACCEPTED MANUSCRIPT
This is the author's peer reviewed, accepted manuscript. However, the online version of record will be different from this version once it has been copyedited and typeset.
PLEASE CITE THIS ARTICLE AS DOI: 10.1063/5.0205876

shows that the ZnO (002) peak position has a systematic shift under the different polarization states of the PMN-PT producing an out-of plane strain on the film, as depicted in Fig. 3c. This strain, ϵ_{zz}, generates an induced polarization on the film via $P_i^{ZnO} = d_{33}\epsilon_{zz}$ (where d_{33} is the piezoelectric coefficient along the c-axis direction) which is added to the spontaneous polarization of ZnO, P_{esp}^{ZnO}, giving a total polarization of [39, 40]: $P_T^{ZnO} = P_{esp}^{ZnO} + P_i^{ZnO}$. From this, the total electric field on the film, ξ_T can be calculated and compared with the internal electric field obtained from the ΔE values, ξ, see lower panel of Fig. 3c. As it can be observed there is a good agreement between both electric fields confirming that the band bending established on the film is generated by the total polarization on the ZnO which in turn is modified by strain due to the piezoelectric effect on the film at the different PMN-PT states. Values of $d_{33} = 1.4\,\mathrm{C\,m^{-2}}$ and $P_{esp}^{ZnO} = -0.016\,\mathrm{C\,m^{-2}}$ have been employed while previous works [39, 59, 60] report $d_{33} = 0.8\text{–}1.4\,\mathrm{C\,m^{-2}}$ and $P_{esp}^{ZnO} = -0.05\,\mathrm{C\,m^{-2}}$. The different values of P_{esp}^{ZnO} can be explained considering that films tend to produce more defects and are less oriented than single crystals decreasing in this way the amplitude of P_{esp}^{ZnO}.

In the sketch of Fig. 4 we have described this phenomenon in the different polarization states. In the unpolarized P^0 state (central panel) $P_T^{ZnO} = P_{esp}^{ZnO}$ and this polarization generates an initial band bending on the film and certain value of E_G. On one hand, as the substrate is brought to the P_r^+ state (left panel), the substrate imposes a compressive (negative) strain along the c-axis of the film increasing the total polarization of ZnO (P_T^{ZnO}) in a quantity $d_{33}\epsilon_{zz}$ in relation to the P^0 state. In this way band bending increases and E_G is reduced in comparison to the unpolarized state. On the other hand, in the P_r^- state (right panel), the substrate imposes a tensile (positive) strain along the c-axis of the film decreasing the total polarization of ZnO in a quantity $d_{33}\epsilon_{zz}$ in relation to the P^0 state. This effect decreases the band bending and increases E_G in comparison to the P^0 state.

The sketch of Fig. 4 also describes why the electrical resistance of the ZnO film increases as the polarization state is changed from P_r^- to P^0 and P_r^+, see Fig. 2c. Assuming that the Fermi energy level, E_F, remains unchanged under the different polarization states and that it is located close to the upper limit of the impurity band [61, 62] (see the P_r^- state in the right panel of Fig. 4) it can be noticed that as band bending is increased (towards the P^0 and P_r^+ states) the fraction of uncovered impurity band above E_F (with an area $1/2(e\xi t/2)(t/2)$ in the energy diagram) increases, increasing in this way the density of impurities that become ionized (i.e. positively ionized oxygen vacancies). Since the confined electrons due to the band bending can be considered as a 2D electron gas [63], their mobility due to the scattering with ionized impurities located on a plane at a distance δ from these carriers is: $\mu^{2D} \propto \delta^3/n_{imp}^{2D}$, where n_{imp}^{2D} is the number

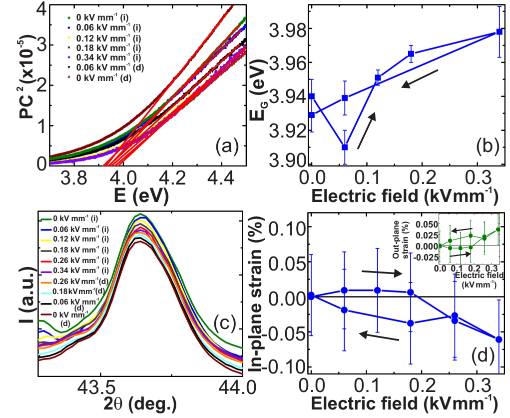

Figure 5. (a) PC^2 spectra of BSO at different applied electric fields following a closed cycle sequence. (i) and (d) means increasing and decreasing voltage respectively. Red lines are corresponding fits. (b) Extracted E_G values as a function of the applied electric field on the substrate following this closed cycle sequence. (c) (002) peak of BSO at different applied electric fields following a similar closed cycle sequence. The curves are vertically shifted for clarity. The inset of (d) shows the out-of-plane strain obtained from these peaks and the main panel of (d) shows the corresponding in-plane strain using the Poisson's formula.

of ionized impurities per unit area [64]. Moreover, taking into account that $n_{imp}^{2D} = \rho_{imp}^{3D} 1/2(e\xi t/2)(t/2)$ (where ρ_{imp}^{3D} is the density of states of the impurity band) the proportionality $\mu^{2D} \propto (e\xi t)^{-1}$ is obtained, suggesting that an increase of band bending decreases mobility and increases the electrical resistance of the ZnO film as the polarization of the PMN-PT substrate is changed from P_r^- to P^0 and P_r^+.

Fig. 5a shows the PC^2 spectra for BSO at different applied electric fields following a closed-cycle sequence. From a linear fitting of these spectra, the corresponding E_G values can be extracted and they are plotted as a function of the electric field in Fig. 5b. As it can be observed, the E_G vs electric field curve is very similar to the electrical resistance one, see Fig. 2d, suggesting that both physical parameters are modified by strain. In order to confirm that, we have measured the electric field dependence of the (002) peak position of BSO, see Fig. 5c. From this peak we have extracted the out-of-plane lattice parameter and the corresponding strain, see inset of Fig. 5d and using the Poisson's formula we have obtained the in-plane strain on the BSO film vs applied electric field curve, see main panel of Fig. 5d. As it can be noticed, an in-plane compressive strain produces an increment of the energy gap and the electrical resistance as it can be observed in Fig. 5b and Fig. 2d while for an in-plane tensile strain both parameters (E_G and resistance) are

AIP Publishing Applied Physics Letters ACCEPTED MANUSCRIPT
This is the author's peer reviewed, accepted manuscript. However, the online version of record will be different from this version once it has been copyedited and typeset.
PLEASE CITE THIS ARTICLE AS DOI: 10.1063/5.0205876

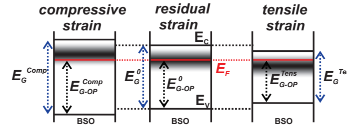

Figure 6. Sketch of the energy diagram for BSO. When an in-plane compressive strain is applied on the BSO film (left panel), an increment of E_G takes place in comparison to the unstrained (or residual strain) case (central panel) while an in-plane tensile strain (right panel) reduces E_G. In all the cases, the Fermi energy level remains unchanged. The optical gap (E_{G-OP}) extracted from the PC spectra is also showed and it is assumed to follow the variations of E_G in all the cases.

reduced.

The sketch of Fig. 6 illustrates the situation for the BSO film. As an in-plane tensile strain is applied on the film (right panel of Fig. 6) there is a reduction of E_G in comparison with the unstrained (or residual strain) situation (central panel) which is reflected in a lower shift of the minimum of the conduction band, E_C, as it was previously reported in other semiconductors [53, 54]. When an in-plane compressive strain is applied on the film (left panel), the opposite situation occurs, that is, there is an upper shift of E_C and an increment of E_G. If the impurity band (blurred black region) is shifted in the same proportion as E_C and assuming that E_F is originally located in the middle of the impurity band and that it is not shifted under the induced strain, the behavior of the electrical resistance under strain (Fig. 2d) can also be understood. Under an in-plane compressive strain (left panel), the uncovered portion of the impurity band above E_F is higher in relation to the unstrained (residual strain) case in an energy $(E_G^{comp} - E_G^0)/2$. Again, this uncovered portion of the impurity band represents extra ionized impurities that are effective for scattering and reducing the electron mobility via $\mu \propto (n_{imp}^{3D})^{-1}$ [65], where n_{imp}^{3D} is the density of these ionized impurities. Since these extra ionized impurities δn_{imp}^{3D} can be written as $\delta n_{imp}^{3D} = \rho_{imp}^{3D}(E_G^{comp} - E_G^0)/2$, an in-plane compressive strain leads to an increase of the electrical resistance in comparison to the unstrained case. In a similar way, an in-plane tensile strain (right panel) leads to a relative decrease of n_{imp}^{3D} and a decrease of resistance in comparison to the unstrained case.

In summary the behavior of the energy gap and the electrical resistance of ZnO and BSO films grown on PMN-PT are modified by an external electric field applied on the substrate. In the case of ZnO this response is controlled by the polarization state of the substrate and the imposed strain on the film that modifies its polarization via the piezoelectric effect. On the other hand, in BSO this response only depends on the strain imposed by the PMN-PT. In the former case, band bending generated by the induced polarization is the responsible of the observed effects while for BSO a shift of the conduction and impurity band caused by the strain explains the modifications of the resistance and the energy gap.

I. ACKNOWLEDGEMENTS

This work was supported by INFINOA-PUE-08 (CONICET), SCAIT- No. E716 and E753, PIP 0057, SNMAG and SINALA facilities. We thank A. M. Lucero Manzano for help with the ToF-SIMS measurements and P. D. Perez for help with the RBS measurements at TANDEM accelerator, and G. Rozas for help with the ellipsometry measurements, all at Centro Atomico Bariloche Argentina. We thank S. Suarez and O. Grizzi for valuable discussions.

II. DATA AVAILABILITY

The data that supports the findings of this study are available from the corresponding author upon reasonable request.

[1] Z. Lei, J. M. Lee, G. Singh, C.I. Sathish, Xueze Chu, A. H. Al-Muhtaseb, A. Vinu, J. Yi, Energy Storage Materials **36**, 514-550 (2021).
[2] J. Heber, Nature **459**, 28-30 (2009).
[3] J. L. MacManus-Driscoll, M. P. Wells, C. Yun, J.-W. Lee, C.-B. Eom and D. G. Schlom, APL Mater. **8** 040904 (2020).
[4] D. H. A. Blank, M. Dekkers, and G. Rijnders, J. Phys. D: Appl. Phys. **47**(3), 034006 (2014)
[5] D. G. Schlom, L.-Q. Chen, X. Pan, A. Schmehl, and M. A. Zurbuchen, J. Am. Ceram. Soc. **91**(8), 2429-2454 (2008)
[6] H. Y. Hwang, Y. Iwasa, M. Kawasaki, B. Keimer, N. Nagaosa and Y. Tokura, Nature Materials **11**, 103-113 (2012).
[7] J. F. Wager, Information Display **32**(1), 16-21 (2016).
[8] J. F. Wager, Information Display **36**, 9-13 (2020).
[9] A. Janotti and C. G. Van de Walle, Phys. Rev. B **76**, 165202 (2007).
[10] D. O. Scanlon, Phys. Rev. B **87**, 161201(R) (2013).
[11] J. Buckeridge, C. R. A. Catlow, M. R. Farrow, A. J. Logsdail, D. O. Scanlon, T. W. Keal, P. Sherwood, S. M.

AIP Publishing Applied Physics Letters ACCEPTED MANUSCRIPT
This is the author's peer reviewed, accepted manuscript. However, the online version of record will be different from this version once it has been copyedited and typeset.
PLEASE CITE THIS ARTICLE AS DOI: 10.1063/5.0205876

Woodley, A. A. Sokol and A. Walsh, Phys. Rev. Mat. **2**, 054604 (2018).

[12] Z. Q. Liu, C. J. Li, W. M. Lu, X. H. Huang, Z. Huang, S. W. Zeng, X. P. Qiu, L. S. Huang, A. Annadi, J. S. Chen, J. M. D. Coey, T. Venkatesan and Ariando, Phys. Rev. X **3**, 021010 (2013).

[13] Y. Liu, C. Ma, Q. Zhang, W. Wang, P. Pan, L. Gu, D. Xu, J. Bao and Z. Dai, Adv. Mater. **31**, 1900062 (2019).

[14] T. Zhao, A. Scholl, F. Zavaliche, K. Lee, M. Barry, A. Doran, M. P. Cruz, Y. H. Chu, C. Ederer, N. A. Spaldin, R. R. Das, D. M. Kim, S. H. Baek, C. B. Eom and R. Ramesh Nature Materials 5, 823-829 (2006).

[15] Y.-M. Kim, A. Morozovska, E. Eliseev, M. P. Oxley, R. Mishra, S. M. Selbach, T. Grande, S. T. Pantelides, S. V. Kalinin and A. Y. Borisevich, Nature Materials 13, 1019-1025 (2014).

[16] C. Ma, Z. Luo, W. Huang, L. Zhao, Q. Chen, Y. Lin, X. Liu, Z. Chen, C. Liu, H. Sun, X. Jin, Y. Yin and X. Li, Nat Commun. **11**, 1439 (2020).

[17] Y. Jiang, E. Parsonnet, A. Qualls, W. Zhao, S. Susarla, D. Pesquera, A. Dasgupta, M. Acharya, H. Zhang, T. Gosavi, C.-C. Lin, D. E. Nikonov, H. Li, I. A. Young, R. Ramesh and L. W. Martin, Nature Materials **21**, 779-785 (2022).

[18] L. Dai, J. Zhao, J. Li, B. Chen, S. Zhai, Z. Xue, Z. Di, B. Feng, Y. Sun, Y. Luo, M. Ma, J. Zhang, S. Ding, L. Zhao, Z. Jiang, W. Luo, Y. Quan, J. Schwarzkopf, T. Schroeder, Z.-G. Ye, Y.-H. Xie, W. Ren and G. Niu, Nat Commun. **13**, 2990 (2022).

[19] C.-L. Jia, K. W. Urban, M. Alexe, D. Hesse and I. Vrejoiu, Science **331** (6023), 1420-1423 (2011).

[20] A. Lipatov, A. Fursina, T. H. Vo, P. Sharma, A. Gruverman and A. Sinitskii, Adv. Electron. Mater. **3**, 1700020 (2017).

[21] B. Radisavljevic, A. Radenovic, J. Brivio, V. Giacometti and A. Kis, Nature Nanotechnology **6**, 147-150 (2011).

[22] Y. Cao, J. Meng, Q. Li, T. Wang, H. Zhu, Q. Sun, D. W. Zhang and L. Chen, Adv. Electron. Mater. **8**, 2200909 (2022).

[23] K. Chatterjee, S. Kim, G. Karbasian, A. J. Tan, A. K. Yadav, A. I. Khan, C. Hu and S. Salahuddin, IEEE Electron Device Lett. **38**, 1379 (2017).

[24] P.-C. Shen, C. Lin, H. Wang, K. H. Teo and J. Kong, Appl. Phys. Lett. 116, 033501 (2020).

[25] M.-K. Kim, I.-J. Kim and J.-S. Lee, ACS Omega 8, 20, 18180-18185 (2023).

[26] R. K. Zheng, Y. Wang, H. L. W. Chan, C. L. Choy and H. S. Luo, Phys. Rev. B **75**, 212102 (2007).

[27] D. Pesquera, E. Khestanova, M. Ghidini, S. Zhang, A. P. Rooney, F. Maccherozzi, P. Riego, S. Farokhipoor, J. Kim, X. Moya, M. E. Vickers, N. A. Stelmashenko, S. J. Haigh, S. S. Dhesi and N. D. Mathur, Nat Commun. **11**, 3190 (2020).

[28] S. Heo, D. Yoonb, S. Yub, J. Sonb and H. M. Jang, J. Mater. Chem. C. **00**, 1-3 (2017).

[29] A. Ahlawat, R. Roth, D. Rata, K. Dorr, A. A. Khan, P. Deshmukh, M. M. Shirolkar, S. Satapathy, R. J. Choudhary and D. M. Phase, Appl. Phys. Lett. **119**, 152901 (2021).

[30] Q.-X. Zhu , M.-M. Yang, M. Zheng, R.-K. Zheng, L.-J. Guo, Y. Wang, J.-X. Zhang , X.-M. Li , H.-S. Luo and X.-G. Li, Adv. Funct. Mater. **25**, 1111-1119 (2015).

[31] L. Che, W.-Y. Zhao, J. Wang, G.-Y. Gao, J.-X. Zhang, Y. Wang, X.-M. Li, S.-X. Cao, X.-G. Li, H.-S. Luo and R.-K. Zheng, ACS Appl. Mater. Interfaces **8**, 26932-26937 (2016).

[32] S. Chen, C. Cao, L. Shen, M. Liu, C. Jiang, Q. Zhan and X. Qiu, Appl. Phys. Lett. **119**, 252401 (2021).

[33] G. Lezier, P. Kolej, J.-F. Lampin, K. Postava, M. Vanwolleghem and N. Tiercelin, Appl. Phys. Lett. **120**, 152404 (2022);

[34] Q. Lu, P. Li, Z. Guo, G. Dong, B. Peng, X. Zha, T. Min, Z. Zhou and M. Liu, Nat. Commun. **13**, 1650 (2022).

[35] V. Iurchuk, J. Bran, M. Acosta and B. Kundys, Appl. Phys. Lett. **122**, 072404 (2023).

[36] G. Bai, Y. Zhang and J. Hao, Sci. Rep. **4**, 5724 (2014).

[37] Y. C. Jiang and J. Gao, Sci. Rep. **4**, 6738 (2014).

[38] W. Zhang, M.-M. Yang, X. Liang, H.-W. Zheng, Y. Wang, W.-X. Gao, G.-L. Yuan, W.-F. Zhang, X.-G. Li, H.-S. Luo, R.-K. Zheng, Nano Energy **18**, 315-324 (2015).

[39] A. Dal Corso, M. Posternak, R. Resta and A. Baldereschi, Phys. Rev. B **50**, 10715 (1994).

[40] B. Meyer and D. Marx, Phys. Rev. B **67**, 035403 (2003).

[41] U. Kim, C. Park, T. Ha, R. Kim, H. S. Mun, H. M. Kim, H. J. Kim, T. H. Kim, N. Kim, J. Yu, K. H. Kim, J. H. Kim and K. Char, APL Materials **2**, 056107 (2014).

[42] U. Kim, C. Park, T. Ha, Y. M. Kim, N. Kim, C. Ju, J. Park, J. Yu, J. H. Kim and K. Char, APL Materials **3**, 036101 (2015).

[43] S. Raghavan, T. Schumann, H. Kim, J. Y. Zhang, T. A. Cain and S. Stemmer, APL Materials **4**, 016106 (2016).

[44] R. R. Reeber, J. Appl. Phys. **41**, 5063-5066 (1970).

[45] A. Bouhemadou, K. Haddadi, Solid State Sciences **12**, 630-636 (2010).

[46] H. J. Kim, J. Kim, T. H. Kim, W.-J. Lee, B.-G. Jeon, J.-Y. Park, W. S. Choi, D. W. Jeong, S. H. Lee, J. Y., T. W. Noh and K. H. Kim, Phys. Rev. B **88**, 125204, (2013).

[47] G. Bridoux, M. Villafuerte, J. M. Ferreyra, N. Bachi, C. A. Figueroa and S. P. Heluani, Phys. Rev. B **92**, 155202 (2015).

[48] G. Bridoux, M. Villafuerte, J. M. Ferreyra, J. Guimpel, G. Nieva, C. A. Figueroa, B. Straube and S. P. Heluani, Appl. Phys. Lett. **112**, 092101 (2018).

[49] G. Bridoux, G. D. Ruano, J. M. Ferreyra and M. Villafuerte, J. Appl. Phys. **127**, 245704 (2020).

[50] G. Bridoux, J. M. Ferreyra, J. Guimpel, G. Nieva and M. Villafuerte, Appl. Phys. Lett. **118**, 132101 (2021).

[51] J. I. Pankove, Optical Processes in Semiconductors (Dover Publications Inc., New York, 1976).

[52] A. Cavallini, L. Polenta, M. Rossi, T. Stoica, R. Calarco, R. J. Meijers, T. Richter and H. Lüth, Nano Lett. **7**, 2166 (2007).

[53] C. P. Kuo, S. K. Vong, R. M. Cohen and G. B. Stringfellow, J. Appl. Phys. **57** (12), 5428 (1985).

[54] C. K. Maiti, Chattopadhyay and L. K. Bera, Strained -Si Heterostructure Field Effect Devices (Taylor and Francis, New York, 2007).

[55] Ü. Özgür, D. Hofstetter and H. MorkoÃ§, Proc. IEEE **98**, 1255 (2010).

[56] Z. Zhang and J. T. Yates Jr., Chem. Rev. 112, 5520 (2012).

[57] J. M. Ferreyra, G. Bridoux, M. Villafuerte, B. Straube, J. Zamora, C. A. Figueroa, S. P. Heluani, Solid State Communications **257**, 42-46 (2017).

[58] J. D. Dow and D. Redfield, Phys. Rev. B **1**, 3358 (1970).

AIP Publishing
Applied Physics Letters ACCEPTED MANUSCRIPT
This is the author's peer reviewed, accepted manuscript. However, the online version of record will be different from this version once it has been copyedited and typeset.
PLEASE CITE THIS ARTICLE AS DOI: 10.1063/5.0205876

[59] F. Bernardini, V. Fiorentini and D. Vanderbilt, Phys. Rev. B **56**, R10024(R) (1997).
[60] S.-H. Park and D. Ahn, Appl. Phys. Lett. **87**, 253509 (2005).
[61] N. Mott and E. Davis, Electronic Processes in Non-Crystalline Materials (University Press, Oxford, 1979).
[62] B. Shklovskii and A. Efros, Electronic Properties of Doped Semiconductors, Solid-State Science **45** (Springer-Verlag, 1984).
[63] J. Betancourt, J. J. Saavedra-Arias, J. D. Burton, Y. Ishikawa, E. Y. Tsymbal and J. P. Velev, Phys. Rev. B **88**, 085418 (2013).
[64] J. H. Davies, The Physics of Low-Dimensional Semiconductors (Cambridge University Press, New York, 1998).
[65] D. Chattopadhyay and H. J. Queisse, Rev. Mod. Phys. **53**, 745 (1981).